

# Evaluation of a Low-Noise, Formate Spiral Bevel Gear Set

David G. Lewicki, Faydor L. Litvin, Ron L. Woods and Alfonso Fuentes

## Management Summary

Studies to evaluate low-noise Formate spiral bevel gears were performed. Experimental tests were conducted on a helicopter transmission test stand. Low-noise, Formate spiral bevel gears were compared to the baseline OH-58D spiral bevel gear design; a high-strength design; and previously tested, low-noise designs (including an original low-noise design and an improved-bearing-contact, low-noise design). Noise, vibration and tooth strain tests were performed.

## Introduction

Spiral bevel gears are used extensively in rotorcraft applications to transfer power and motion through non-parallel shafts. In helicopter applications, spiral bevel gears are used in main-rotor and tail-rotor gearboxes to drive the rotors. In tilt-rotor applications, they are used in interconnecting drive systems to provide a mechanical connection between two prop rotors should one engine become inoperable. Spiral bevel gears have had considerable success in these applications, yet they remain a main source of vibration and noise in gearboxes. Also, higher strength and lower weight are required to meet the needs of future aircraft.

Previous studies on gears with tooth fillet and root modifications to increase strength were reported, as well as gears with tooth surfaces designed for reduced transmission errors (Refs. 1–2). The teeth were designed using the methods of Litvin and Zhang (Ref. 3) to exhibit a parabolic function of transmission error at a controlled low level (8 to 10 arc sec). This eliminated discontinuities in transmission error, thus reducing the vibration and noise caused by the mesh. The new tooth geometries for this design were achieved through slight modification of the machine tool settings used in the manufacturing process of the pinion. The design analyses addressed tooth generation, tooth contact analysis, transmission error prediction and effects of misalignment (Refs 3–6). The results from these tests showed a significant decrease in spiral bevel gear noise, vibration and tooth fillet stress. However, a hard-line condition (concentrated wear lines) was present on the pinion tooth flank area. A hard-line condition could possibly lead to premature failure such as early pitting/surface fatigue, excessive wear, or scoring, and should be avoided in a proper gear design. Subsequent analyses and tests were performed to improve the gear tooth contact (eliminate the hard-line) while maintaining low noise, vibration and fillet stress (Refs. 7–8).

Spiral bevel gears in current helicopter applications (as well as the low-noise, high-strength designs described above) are manufactured using a face milling process (Ref. 9). The gear material is carburized, and the final manufacturing process—grinding—produces extremely high-precision tooth surfaces. In the face milling process, a circular cutter (or grinding wheel) is designed and set into position, relative to the gear blank, to cut the correct spiral and pressure angles at a specific point on the tooth. The cutter then sweeps out the tooth form as it rotates about its axis (Ref. 9). This relative motion between the cutter and the gear blank is a time-consuming and costly process, but is required to produce accurate teeth.

An alternative manufacturing approach is the Formate process (Ref. 10). Similar to the face milling process, the cutter/grinding wheel is positioned relative to the gear blank so that the correct spiral and pressure angles will be produced. The gear blank, however, is held stationary and a tooth slot is form-cut by in-feeding the cutter without relative motion between the cutter and gear blank. This subtle-yet-important difference substantially reduces the time and cost needed for manufacture. The resulting tooth surface from the Formate process is a straight-tooth, cross-sectional profile. Thus, the process is only applicable to the gear—and not the pinion—in order to achieve proper meshing and a good contact pattern. This still provides significant manufacturing cost reduction benefits, as the gear customarily has a greater number of teeth than the pinion.

Analyses were performed to apply the low-noise design methodology described above to the Formate manufacturing process (Refs. 11–12). Again, the analysis addressed tooth generation, tooth contact analysis, transmission error prediction and effects of misalignment. A Formate spiral bevel gear, along with a specially generated pinion matched for low noise, were fabricated and tested. The objective of this

report is to describe the results of the experiments in evaluating the low-noise, Formate spiral bevel gear set design. Experimental tests were performed on the OH-58D helicopter main-rotor transmission in the NASA Glenn 500-hp helicopter transmission test stand. The low-noise, Formate spiral bevel gear design was compared to: a baseline OH-58D spiral bevel gear design; a high-strength design; and previous low-noise designs. Noise, vibration and tooth strain test results are presented.

### Apparatus

**OH-58D main-rotor transmission.** The OH-58 Kiowa is an Army single-engine, light observation helicopter—an advanced version developed under the Army Helicopter Improvement Program (AHIP). The OH-58D main-rotor transmission is shown in Figure 1. It is currently rated at maximum continuous power of 410 kW (550 hp) at 6,016 rpm input speed, with the capability of 10 sec torque transients to 475 kW (637 hp), occurring at a maximum of once per hour. The main-rotor transmission is a two-stage reduction gearbox with an overall reduction ratio of 15.23:1. The first stage is a spiral bevel gear set with a 19-tooth pinion that meshes with a 62-tooth gear. Triplex ball bearings and one roller bearing support the bevel pinion shaft. Duplex ball bearings and one roller bearing support the bevel gear shaft. Both pinion and gear are straddle-mounted.

A planetary mesh provides the second reduction stage. The bevel gear shaft is splined to a sun gear shaft. The 27-tooth sun gear meshes with four 35-tooth planet gears, each supported with cylindrical roller bearings. The planet gears mesh with a 99-tooth, fixed ring gear splined to the transmission housing. Power is taken out through the planet carrier splined to the output mast shaft. The output shaft is in turn supported on top by a split, inner-race ball bearing, and on the bottom by a roller bearing. The 62-tooth bevel gear also drives a 27-tooth accessory gear. The accessory gear runs an oil pump—which supplies lubrication through jets and passageways located in the transmission housing—as well as a hydraulic pump for aircraft controls.

**Spiral bevel test gears.** Five different spiral bevel pinion and gear designs were compared. The first design was the baseline and used the current geometry of the OH-58D design. Table 1 lists basic design parameters. The reduction ratio of the bevel set is 3.26:1. All gears were made using standard aerospace practices by which the surfaces were carburized and ground. The material used for all test gears was X-53 (AMS 6308). Two sets of the baseline design were tested (Ref. 1). The second spiral bevel design was an increased-strength design. The configuration was identical to the baseline except that the tooth fillet radius of the pinion was increased by a factor of approximately two. Also, the tooth fillet radius of the gear was slightly increased (approximately 1.16 times the baseline) and made full-fillet. Tooth fillet radii larger than those on conventional gears were made possible by advances in spiral bevel gear grinding technology. Advanced gear grinding was achieved through redesign of a

current gear grinder and the addition of computer numerical control (CNC) (Ref.13). Two sets of the increased-strength design were tested (Ref.1).

The third spiral bevel design was a low-noise design. The low-noise design was identical to the increased-strength design, except that the pinion teeth were slightly altered to reduce transmission error. The gear member was the same as in the increased-strength design. The low-noise design was based on the idea of local synthesis that provided the following conditions of meshing and contact at the mean contact point (Ref. 3): a) the required gear ratio and its derivative, b) the desired direction of the tangent to the contact path, and c) the desired orientation and size of the major axis of the instantaneous contact ellipse. The local synthesis was complemented by a tooth contact analysis (Ref. 3). Using this approach, the machine tool settings for reduced noise were determined. As with the high-strength design, precise control of the manufactured tooth surfaces was made possible by advances in the final grinding operation machine tool (Ref. 13). Further information on the low-noise design can be found in References 1–4. In summary, the effect of the topological change in the low-noise design was a reduction in the overall crowning of the tooth, leading to an increase in contact ratio and reduced transmission error.

Two sets of a first attempt at a low-noise design were tested (Ref. 1); this included two low-noise pinions and two gear members that were the same as the high-strength design.

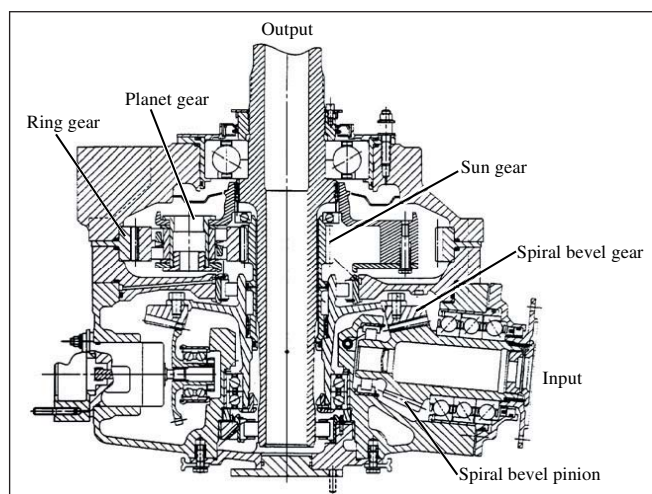


Figure 1—OH-58D helicopter main-rotor transmission.

Table 1. Baseline Spiral-bevel gear parameters of the OH-58D main-rotor transmission.

pinion, number of teeth	19
gear, number of teeth	62
Module, mm (diametral pitch, in <sup>-1</sup> )	4.169 (6.092)
Pressure angle, deg	20
Mean spiral angle, deg	35
Shaft angle, deg	95
Face width, mm (in.)	36.83 (1.450)

In addition, one low-noise pinion with 0.050" TOPREM, one low-noise pinion with 0.090" TOPREM and one low-noise pinion with 0.120" TOPREM were tested (Ref. 8). TOPREM is the decrease in the pressure angle at the tip of the grinding wheel used on the pinion during final machining. This decrease in pressure angle causes more stock to be removed in the flank portion of the tooth to prevent interference with the top of the gear member during operation. The 0.050", 0.090" and 0.120" designations refer to the depth of modification along the blade cutting edge.

The fourth spiral bevel design was an improved-bearing-contact, low-noise design. This new design was in general based on the principles of the previous low-noise design, but also included an improved iterative approach balancing low-transmission errors for reduced noise with tooth contact analysis to avoid adverse contact and concentrated wear conditions (Ref. 7). In addition, modified roll was used in the pinion generation, and finite element analysis was used to evaluate stress and contact conditions. One low-noise, improved-bearing-contact pinion was tested (Ref. 8).

Lastly, the fifth design tested was a 62-tooth, spiral bevel gear manufactured using the Formate process. The 19-tooth, spiral-bevel pinion was manufactured using the conventional, face-milled grinding process. The gear set was designed to reduce transmission error, vibration, noise and stress, as well as to provide proper tooth contact (Refs. 11–12). One Formate set was tested, and the results are compared to the

previously published tests.

#### **NASA Glenn 500-hp helicopter transmission test stand.**

The OH-58D transmission was tested in the NASA Glenn 500-hp helicopter transmission test stand (Fig. 2). The test stand operates on the closed-loop—or torque-regenerative—principle. Mechanical power re-circulates through a closed loop of gears and shafting, part of which is the test transmission. The output of the test transmission attaches to the bevel gearbox. The output shaft of the bevel gearbox passes through a hollow shaft in the closing-end gearbox and connects to the differential gearbox. The output of the differential attaches to the hollow shaft in the closing-end gearbox. The output of the closing-end gearbox connects to the speed increaser gearbox. The output of the speed increaser gearbox attaches to the input of the test transmission, thereby closing the loop.

A 149-kW (200-hp), variable-speed, direct-current (DC) motor powers the test stand and controls the speed. The motor output attaches to the closing-end gearbox. The motor replenishes losses due to friction in the loop. An 11-kW (15-hp) DC motor provides the torque in the closed loop. This motor drives a magnetic particle clutch. The clutch output does not turn, but it exerts a torque. This torque is transferred through a speed reducer gearbox and a chain drive to a large sprocket on the differential gearbox. The torque on the sprocket applies torque in the closed loop by displacing the gear attached to the output shaft of the bevel gearbox with respect to the gear connected to the input shaft of the closing-end gearbox. This is done within the differential gearbox by use of a compound planetary system where the planet carrier attaches to the sprocket housing. The magnitude of torque in the loop is adjusted by changing the electric field strength of the magnetic particle clutch.

A mast shaft loading system in the test stand simulates rotor loads imposed on the OH-58D transmission output mast shaft. The OH-58D transmission output mast shaft connects to a loading yoke. Two vertical-load cylinders connected to the yoke produce lift loads. A 14,000-kPa (2,000-psig) nitrogen gas system powers the cylinders. Pressure regulators connected to the nitrogen supply of each of the load cylinders adjust the magnitude of lift. Note that in the OH-58D design, the transmission at no-load is misaligned with respect to the input shaft. At 18,309 N (4,116 lb) mast lift load, the elastomeric corner mounts of the OH-58D transmission housing deflect such that the transmission is properly aligned with the input shaft. (In the actual helicopter, this design serves to isolate the airframe from the rotor vibration).

The test transmission input and output shafts have speed sensors, torque meters, and slip rings. Both load cylinders on the mast yoke are mounted to load cells. The 149-kW (200-hp) motor has a speed sensor and a torque meter. The magnetic particle clutch has speed sensors on the input and output shafts and thermocouples. An external oil-water heat exchanger cools the test transmission oil. A facility oil-pumping and cooling system lubricates the differential,

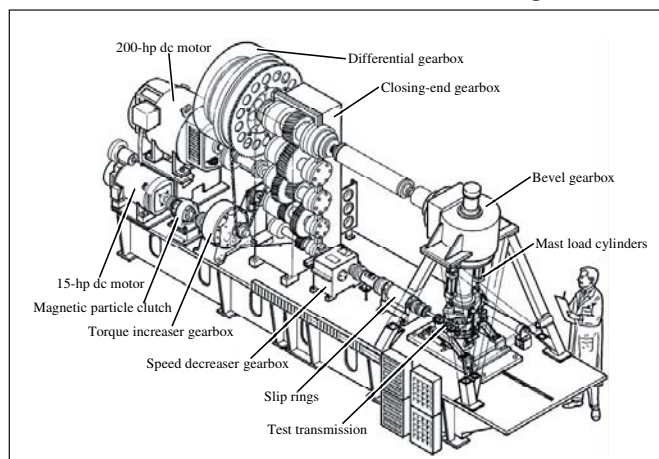


**Figure 2—NASA Glenn 500-hp helicopter transmission test facility.**

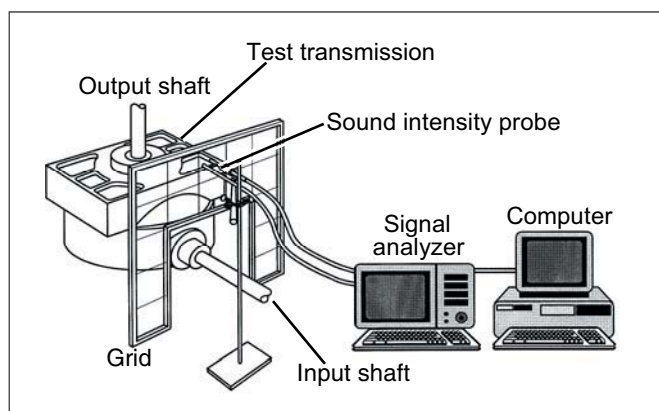


**Figure 3—Sound intensity measurement system.**



closing-end, speed increaser and bevel gearboxes. The facility gearboxes have accelerometers, thermocouples and chip detectors for health and condition monitoring.

### Test Procedure

From the previous studies (Refs.1–2), two sets of the baseline design (each set consisting of a pinion and gear), two sets of the high-strength design and two sets of the original low-noise design were manufactured and tested. Note that the gear members for the high-strength set and original low-noise set were the same gear geometry (same manufacturing settings). There were four of these gear members manufactured—two for the high-strength set and two for the low-noise set. Again, these gears differed from the gear member of the baseline set due to the increased fillet radius and full fillet. Also from previous studies (Ref. 8), three additional, low-noise design pinions with various TOPREM modifications were manufactured and tested. These pinions meshed with one of the gear members of the original low-noise set for all of their tests. Also, one improved-bearing-contact, low-noise design pinion was manufactured and tested (Ref. 8). This pinion meshed with one of the gear members of the high-strength set for all of its tests.

As a summary, noise and vibration tests were performed on all pinions and gears manufactured. In addition, one set of each design was instrumented with strain gages, and strain tests were performed on these. (Again, the improved-bearing-contact, low-noise design pinion meshed with the instrumented gear member of the high-strength set for its strain tests.) A description of the instrumentation, test procedure and data reduction procedure follows.

**Noise tests.** Acoustic intensity measurements were performed using the two-microphone technique. The microphones used had a flat response ( $\pm 2$  dB) up to 5,000 Hz and a nominal sensitivity of 50 mV/Pa. The microphones were connected to a spectrum analyzer, which computed the acoustic intensity from the imaginary part of the cross-power spectrum. Near the input region of the OH-58D transmission, a grid was installed which divided the region into 16 areas (Fig. 3). For each test, the acoustic intensity was measured at the center of each of the 16 areas. Only positive acoustic intensities (noise flowing out of the areas) were considered. The acoustic intensities were then added together and multiplied by the total area of the grids to obtain sound power of the transmission input region.

At the start of each test, the test transmission oil was heated using an external heater and pumping system. For all the tests, the oil used conformed to a DOD-L-85734 specification. Once the oil was heated, the transmission input speed was increased to 3,000 rpm, a nominal amount of torque was applied, and mast lift load was applied to align the input shaft (18,310 N, 4,120 lb). The transmission input speed and torque were then increased to the desired conditions. The tests were performed at 100 percent transmission input speed (6,016 rpm), and torques of 50, 75, 100 and 125 percent of maximum design. The transmission oil inlet temperature was

set at 99° C (210° F). After the transmission oil outlet stabilized (which usually required about 20 min), the acoustic intensity measurements were taken. The time to obtain the acoustic intensity measurements of the 16 grid points at a given test condition was about 30 minutes. For each acoustic intensity spectrum at a grid point, 100 frequency-domain averages were taken. This data was collected by a computer. The computer also computed the sound power spectrum of the grids after all the measurements were taken.

**Vibration tests.** Eight piezoelectric accelerometers were mounted at various locations on the OH-58D transmission housing (Fig. 4). The accelerometers were located near the input spiral bevel area (accelerometers 1 and 2, measuring radially to the input shaft), the ring gear area (accelerometers 3 and 4, measuring radially to the planetary) and on the top cover (accelerometers 5 to 8, measuring vertically). All accelerometers had a 1- to 25,000-Hz ( $\pm 3$  dB) response, 4 mV/g sensitivity and integral electronics. Figure 5 shows a photograph of the noise and vibration test setup.

The vibration tests were performed in conjunction with the noise tests. For the previous studies (Refs. 1, 2 and 8), the vibration data were recorded on tape and processed off-line after collecting the acoustic intensity data for a given test. The vibration data were later analyzed using time averaging. Here, the vibration data recorded on tape were input to a signal analyzer along with a tach pulse from the transmission

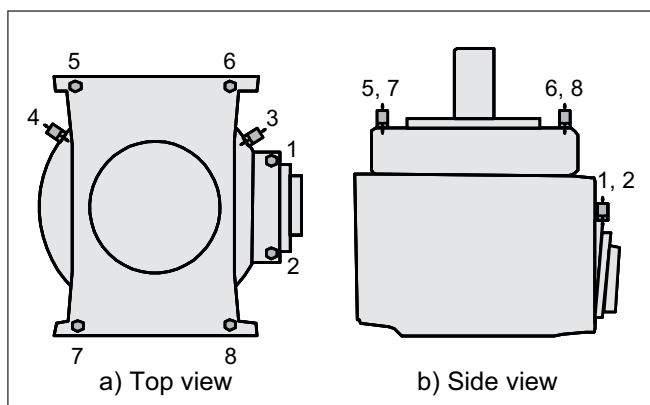


Figure 4—Accelerometer locations on OH-58D transmission.



Figure 5—Noise/vibration test setup.

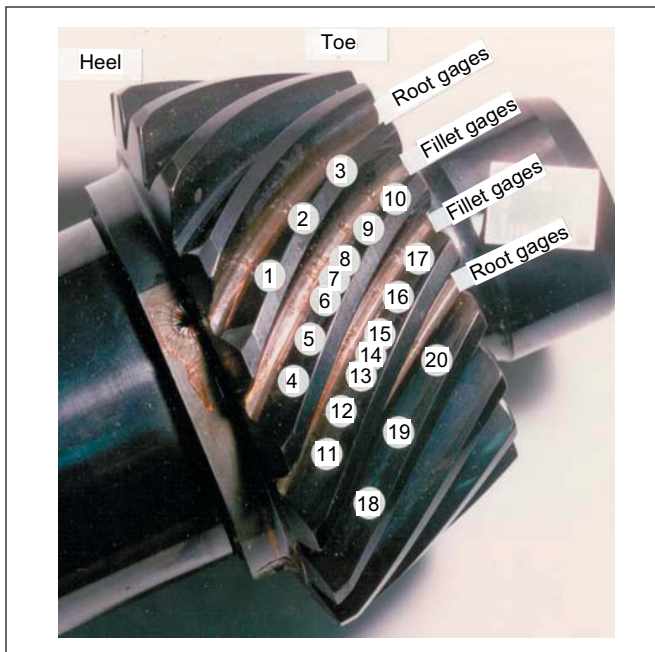


Figure 6—Strain gage locations on spiral bevel pinion.

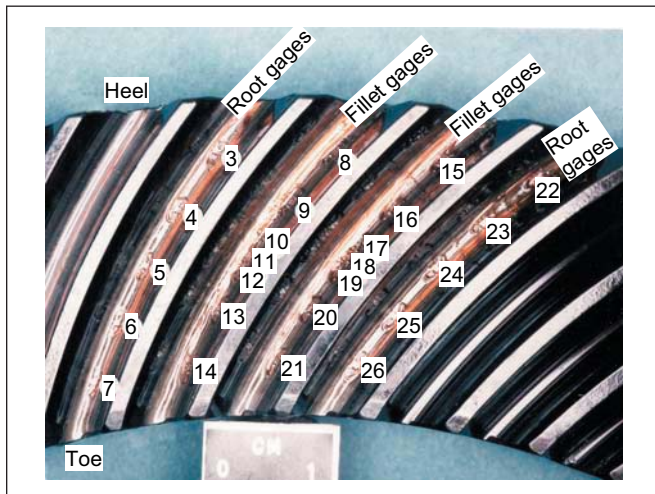


Figure 7—Strain gage locations on spiral bevel gear.



Figure 8—Static strain test setup.

input shaft. The signal analyzer was triggered from the tach pulse to read the vibration data when the transmission input shaft was at the same position. The vibration signal was then averaged in the time domain using 100 averages. This technique removed all the vibration which was not synchronous to the input shaft. Before averaging, the major tones in the vibration spectrum of the OH-58D baseline design were the spiral bevel and planetary gear fundamental frequencies and harmonics. Time averaging removed the planetary contribution, leaving the spiral bevel contribution for comparing the different design configurations.

For the current Formate tests, this above procedure was performed in real time using a computer, and the tape recording was not used. Due to limitations of the number of input channels available for the computer, only seven of the eight accelerometers were processed for the Formate tests. Accelerometers 1–6 and 8 were processed; accelerometer 7 was not.

**Strain tests.** Twenty strain gages were mounted on the spiral bevel pinions for one set of each of the five designs (Fig. 6). Twenty-six gages were mounted on the spiral bevel gears (Fig. 7). Gages were positioned across the tooth face widths with some in the fillet area and some in the root area of the teeth. The fillet gages were placed on the drive side of two adjacent teeth. The fillet gages were also positioned at a point on the tooth cross-section where a line at a 45° angle with respect to the tooth centerline intersects the tooth profile. The fillet gages were placed there to measure maximum tooth-bending stress. (Previous studies on spur gears showed that the maximum stresses were at a line 30° to the tooth centerline (Ref. 14). Forty-five degrees was chosen for the current tests to minimize the possibility of the gages being destroyed due to tooth contact. In addition to maximum tensile stresses, root stresses can become significant in lightweight, thin-rimmed aerospace gear applications (Ref. 15). Thus, root gages were centered between teeth in the root to measure gear rim stress. Tooth fillet and root gages were placed on successive teeth to determine loading consistency. The grid length of the gages was 0.381 mm (0.015 in.) and the nominal resistance was 120  $\Omega$ . The gages were connected to conditioners using a Wheatstone bridge circuitry and quarter-bridge or half-bridge arrangements. (Half-bridge arrangements were used with an adjustable resistor for cases where a gage would not balance in the quarter-bridge arrangement.)

Static strain tests were performed on both the spiral bevel pinions and gears. A crank was installed on the transmission input shaft to manually rotate the shaft to the desired position. A sensor was installed on the transmission input shaft to measure shaft position. At the start of a test, the transmission was completely unloaded and the strain gage conditioners were zeroed. Conditioner spans were then determined using shunt calibrations. The transmission was loaded (using the facility closed-loop system) to the desired torque, the shaft was positioned, and the strain readings along with shaft positions were obtained using a computer. This was done for



a variety of positions to get strain as a function of shaft position for the different gages. At the end of a test, the transmission was again completely unloaded and the conditioner zeroes were checked for drift. A photograph of the static strain setup is shown in Figure 8.

Dynamic strain tests were performed only on the spiral bevel pinions. The pinion gages were connected to slip rings mounted on the input shaft. (A slip ring assembly for the spiral bevel gear was unavailable, and thus, dynamic strain tests of the gear were not performed.) The test procedure was basically the same as the noise and vibration tests, except that the transmission was not run as long in order to maximize strain gage life. A photograph of the dynamic strain setup is shown in Figure 9. The dynamic strain data were digitized into a computer and time-averaged in a manner similar to the vibration data. This procedure was used to remove random slip ring noise.

### Results and Discussion

**Noise tests.** In inspecting the frequency content of the noise data, the sound power at the meshing frequency was a dominant noise source. Figure 10 depicts sound power as a function of torque. The sound power is the sum of the sound power at the spiral-bevel meshing frequency (1,905 Hz) and its first harmonic (3,810 Hz). As interpreted from the figure, the data is divided into three groups.

The first group is the circles and squares, which are the baseline and increased strength designs. The sound power (i.e., noise from the bevel gear mesh) for these designs shows a slight increase with torque. They give about the same trend with approximately 5 dB of scatter. This is expected since the bevel pinion and gear tooth geometries for this group were identical except for the fillet region.

The second group is the upward-facing triangles, which are the original low-noise designs, with and without TOPREM. These data show a significant decrease in noise, especially at the 100% torque condition (about 16 dB). They also show about the same trend with approximately 2 to 8 dB of scatter.

The third group is the solid diamonds and the downward-facing triangles, which are the data from the improved-bearing-contact, low-noise design and Formate design. The sound power from these designs is nearly constant with torque. The improved-bearing-contact, low-noise design shows a decrease in noise from the baseline design (about 7dB at 100% torque), but not as much reduction as the previous low-noise designs. The formate design also shows a slight decrease in noise from the baseline design (about 5dB at 100% torque).

**Vibration tests.** Figure 11 depicts the results from the vibration tests. Shown is acceleration as a function of torque for seven accelerometers mounted on the OH-58 transmission housing. Again, the acceleration was time-averaged with respect to the input shaft to remove all non-synchronous vibration. Upon inspection of the frequency content of the data, the majority of the time-averaged vibration stemmed



Figure 9—Dynamic strain test setup.

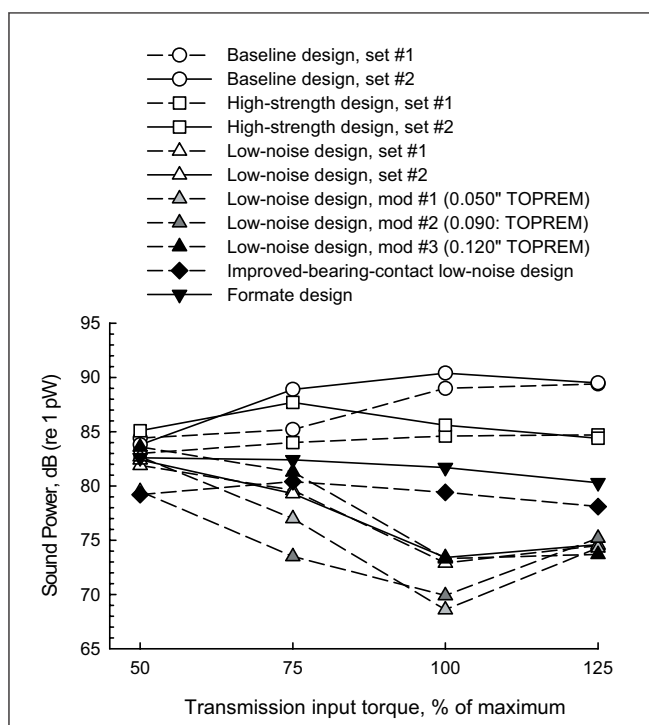


Figure 10—Sound power at spiral-bevel mesh frequencies.

from the spiral bevel mesh. The data points in the figure are the root-mean-square (rms) values of the time-averaged vibration time traces. In general, each figure can be divided into two groups: 1) baseline and high-strength designs (circles and squares); and 2) low-noise and Formate designs (triangles and diamonds). As with the noise results, there was a significant reduction in vibration for the low-noise designs compared to the baseline. For accelerometers 1, 4, 5, 6 and 8, the vibration for all the low-noise and Formate designs is basically lumped together with a scatter of about 3–5 g's. In general, the Formate design gave the same benefit in reduced vibration as that of the previously tested low-noise designs. As with the noise test results, the vibration for the Formate design was fairly constant with torque.

**Strain tests.** Results of the static strain tests at 100% torque for the strain gages are shown in Figures 12–15.

Shown is stress versus pinion shaft position for all gages of the baseline, high-strength, low-noise and Formate designs. Since the strain in the tooth fillet is mostly uniaxial and in the tangential direction of the tooth face (Ref. 16), the stress was calculated by multiplying the measured strain by the modulus of elasticity (30 x 106 psi for steel). For the pinion fillet gages (Fig. 12), the figure depicts results from gages on adjacent gear teeth (gages 4 and 11, 5 and 12, and 6 and 13) for the seven positions along the gear tooth face width. Gages 4 and 11 correspond to positions at the heel of the

pinion, and gages 10 and 17 correspond to positions at the toe of the pinion. The gages show typical results of a driving pinion member rolling through mesh. As it does so, it first sees a small amount of compression in the fillet when the tooth ahead of the strain-gaged tooth is in contact with the driven gear. As the pinion rolls further through mesh, the strain-gaged tooth is in contact with the driver and the fillet region sees tensile stress. At the maximum stress, the strain-gaged tooth is loaded in single-tooth contact. (Note that cases where data are missing from the figure—baseline

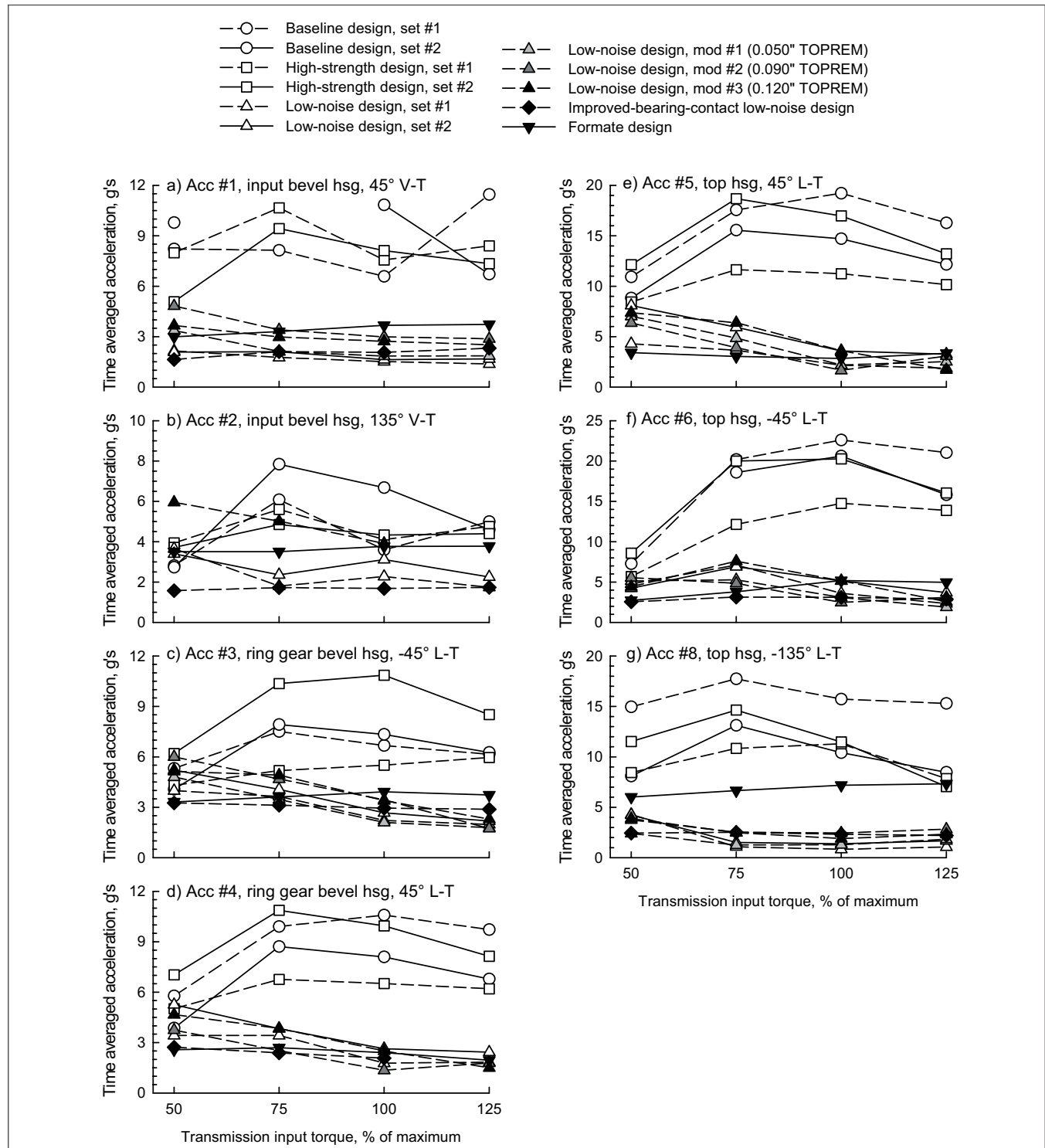


Figure 11—Vibration results.

design gages 4, 5, 8, 9 and 10, as examples—were due to faulty gages.

Figure 16 shows the maximum and minimum stresses as a function of position along the gear tooth face width. For the pinion fillet gages at 100% torque (Figs. 12 and 16a), the maximum tensile stress occurred at the middle of the tooth face width for the baseline and high-strength designs—gage 6, 7, 13 and 14 regions. It should be noted here that gages 6–8 and 13–15 were located as close to each other, respectively, as possible). The minimum stress (maximum com-

pression) for these designs occurred slightly to the heel side of the middle of the tooth face width. The maximum alternating stress occurred at the same location of the maximum tensile stress, where the alternating stress is defined as the maximum stress minus the minimum stress for a given gage position. For the Formate design, maximum values of the stresses (tensile, compressive, alternating) shifted significantly toward the heel, compared to the baseline design. This was also the case for the improved-bearing-contact, low-noise design. For the original low-noise design, maxi-

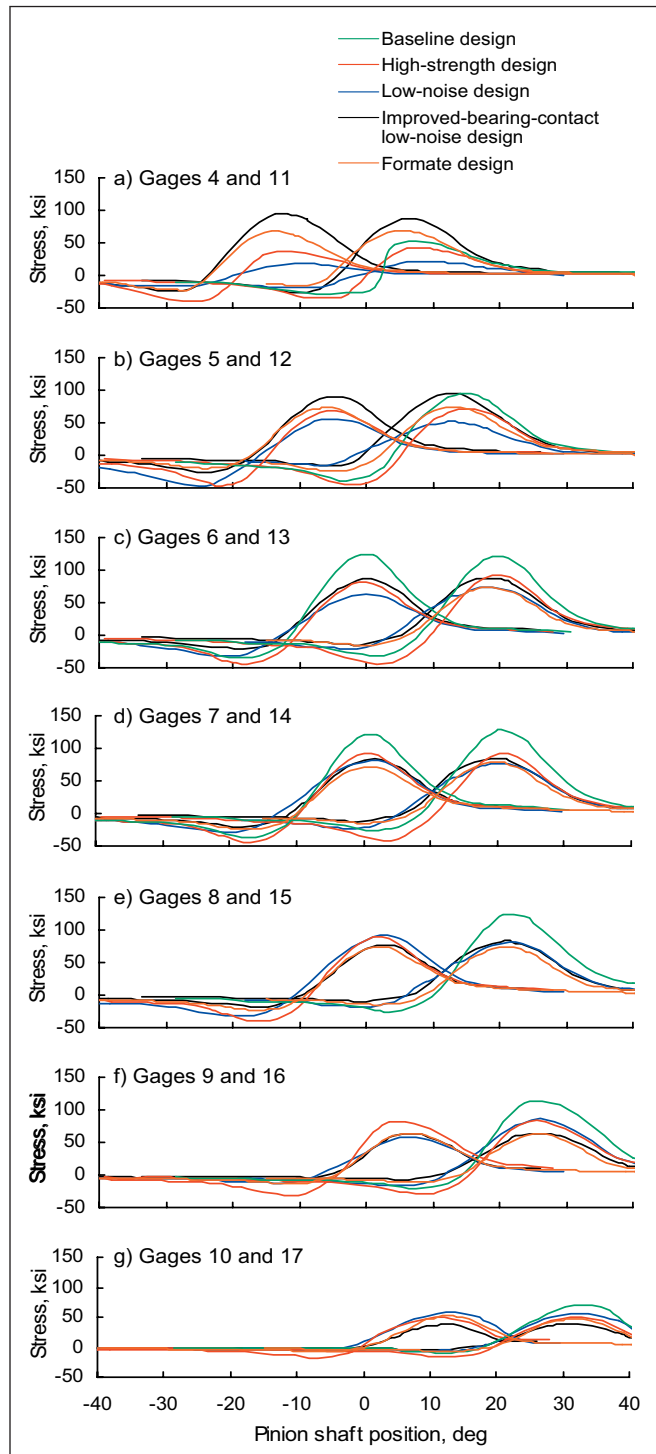


Figure 12—Results from static strain tests, pinion fillet gages, 100% torque (refer to Fig. 8 for strain gage locations).

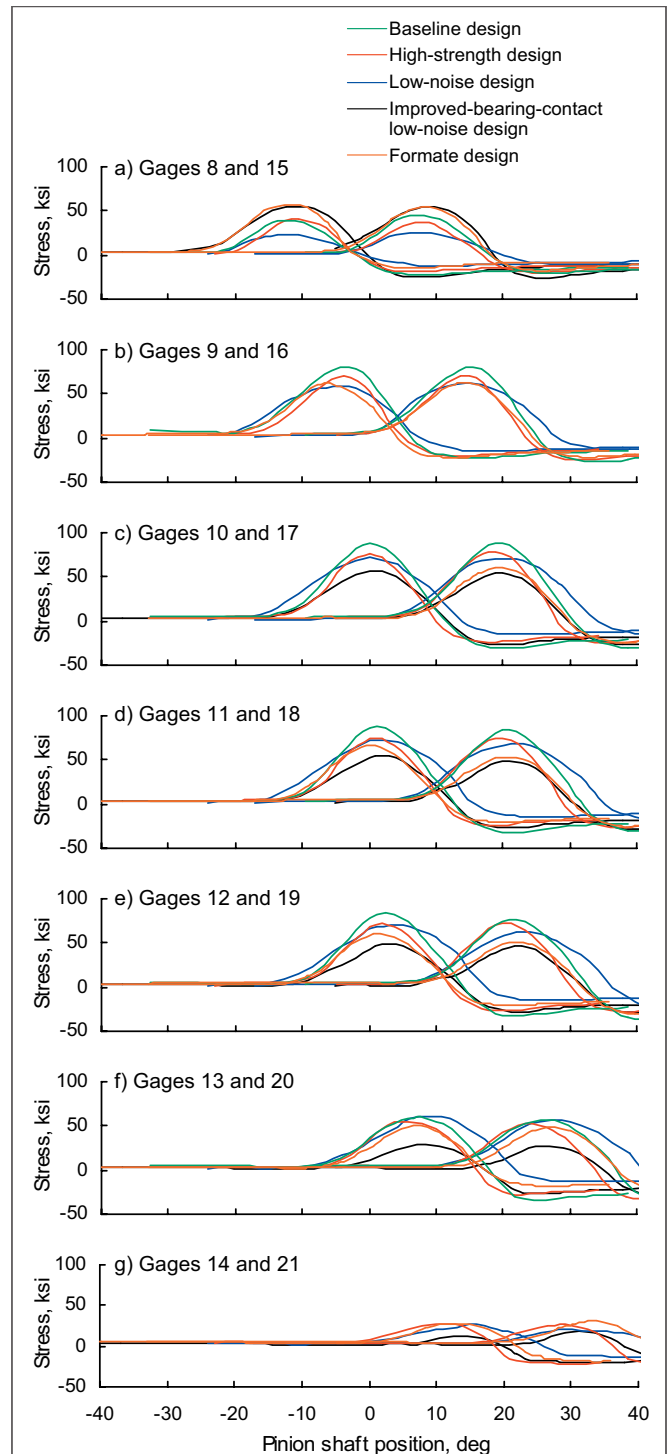


Figure 13—Results from static strain tests, gear fillet gages, 100% torque (refer to Fig. 7 for strain gage locations).



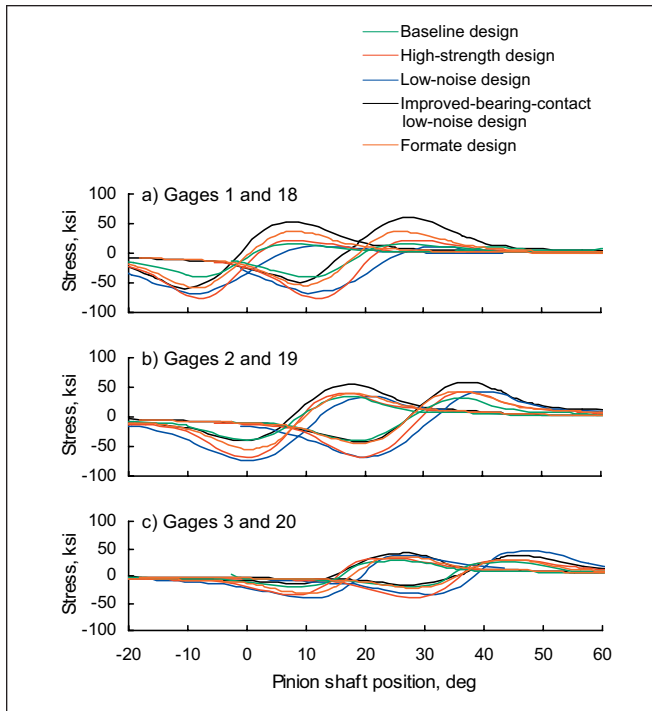


Figure 14—Results from static strain tests, pinion root gages, 100% torque (refer to Fig. 8 for strain gage locations).

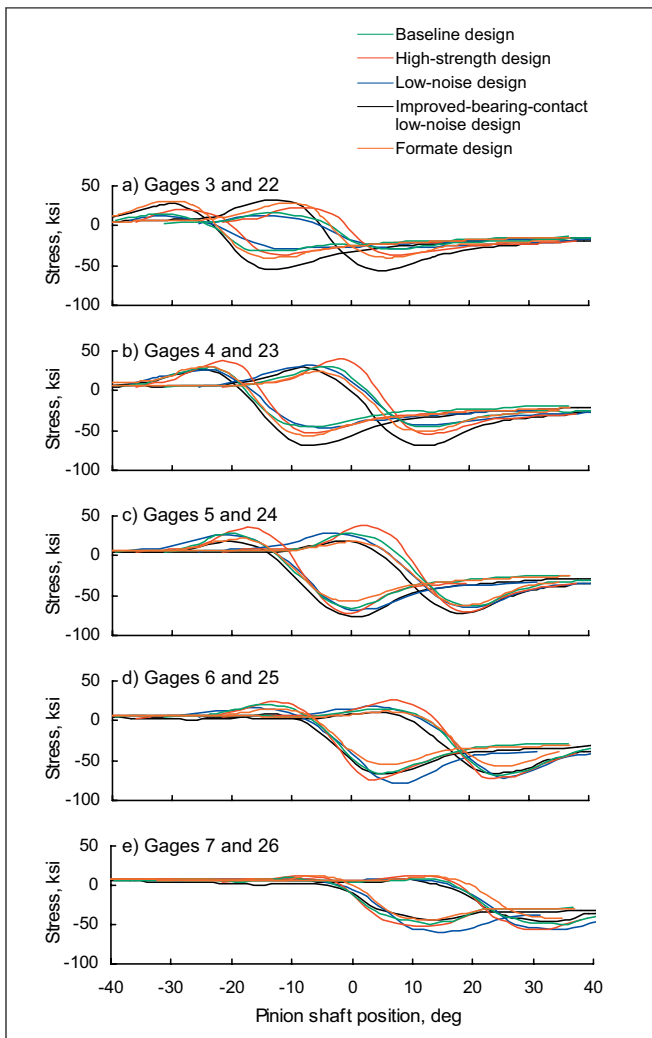


Figure 15—Results from static strain tests, gear root gages, 100% torque (refer to Fig. 8 for strain gage locations).

imum values of the stresses (tensile, compressive, alternating) shifted only slightly toward the toe, compared to the baseline design. Table 2 lists the values of the maximum, minimum and alternating stresses of the various designs tested at 100% torque. It should be noted that the values listed in the table were the average of the two rows of the corresponding gages. In all cases, the change column compares the stress to the baseline design. From Table 2a, there was a significant reduction in pinion fillet maximum tensile stress of the Formate, high-strength and original low-noise designs, compared to the baseline. There was less of a reduction for the improved-bearing-contact, low-noise design, but it was still significant.

For the gear fillet gages (Fig. 13), the shapes of the stress-position traces look similar to that of the pinion, except that the fillet compression occurs after the tension. This is because the tooth ahead of the strain-gage tooth sees contact with the driver member after the strain-gaged tooth is in contact. For the baseline design, high-strength design and original low-noise design, the maximum tensile stresses occurred at the middle of the tooth face width (Figs. 13 and 16b). For the Formate and improved-bearing-contact, low-noise designs, the maximum tensile stress shifted toward the heel. From Table 2b, there was a significant reduction in gear fillet maximum tensile stress for the Formate, high-strength, and all low-noise designs, compared to the baseline. The greatest benefit was from the improved-bearing-contact, low-noise design. Also, note that the magnitude of gear fillet tensile stresses was significantly lower than that of the pinion.

For the pinion root gages (Fig. 14), the stress-position traces were different than the fillet gages in that the maximum compression was nearly twice as great as the maximum tension. However, the magnitude of the maximum tension was significantly less than that in the fillet. Note that although the root gages were physically located three teeth apart (Fig. 6), they are plotted in Figure 14 as if they were on adjacent teeth. As with the fillet gages, the maximum stresses (tensile and alternating) occurred at the middle of the tooth face width for the baseline design, high-strength design and original low-noise design, and shifted toward the heel for the Formate and improved-bearing-contact, low-noise designs (Figs. 14 and 16c). The same trend was observed for the gear root gages (Figs. 15 and 16d). The maximum tensile stress in the pinion root significantly increased for the Formate, high-strength and original low-noise designs, compared to the baseline (Table 2c). The maximum tensile stress in the pinion root drastically increased for the improved-bearing-contact, low-noise design, compared to the baseline. The alternating stresses in the pinion root of the high-strength, and all low-noise designs increased about the same amount, compared to the baseline, whereas the increase was less for the Formate design. The maximum tensile stress in the gear root significantly increased for the high-strength design—compared to the baseline—but stayed the same for

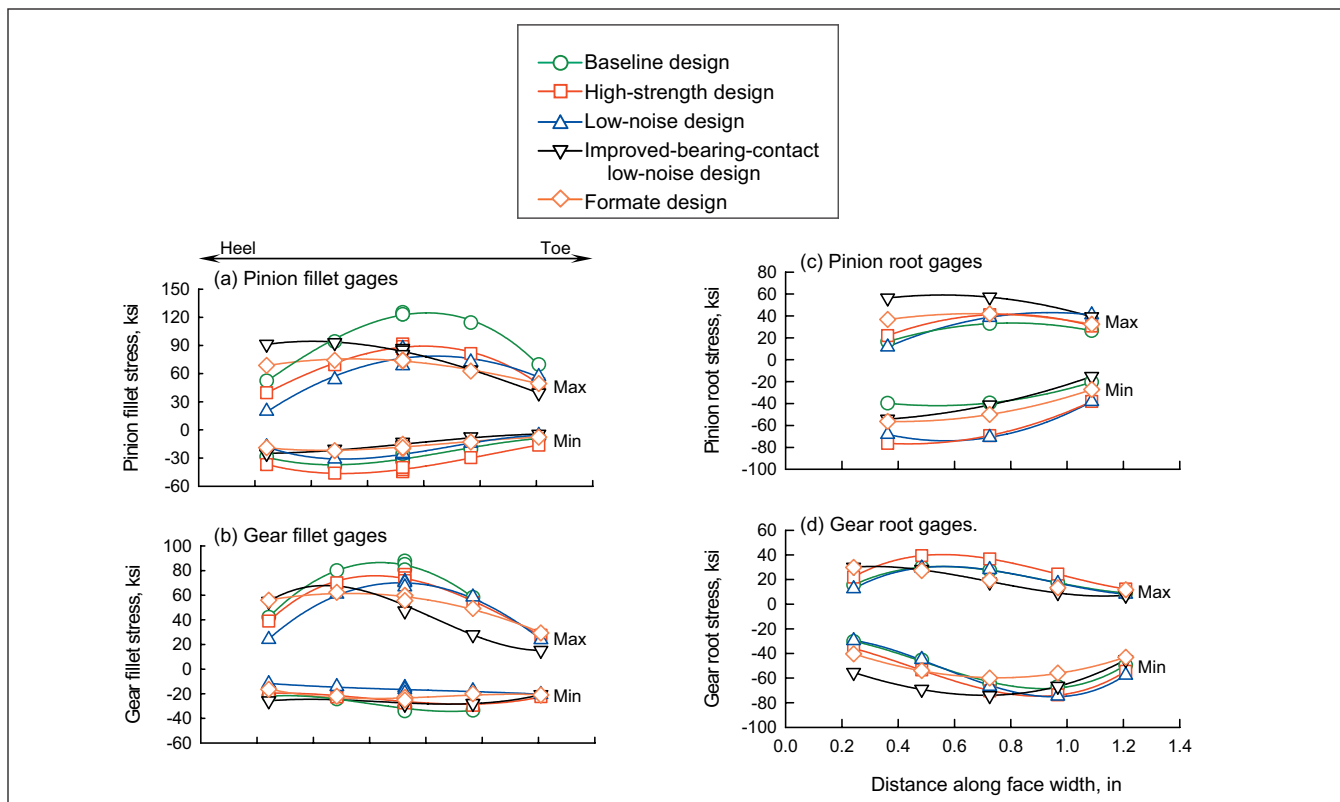


Figure 16—Maximum and minimum gear tooth stress distribution along tooth face width, static strain tests.

Table 2. Comparison of Formate design to previously tested designs, static strain test results at 100% torque.

a) Pinion fillet gages	Max Stress	Change	Min Stress	Change	Alt Stress	Change
	(ksi)	(%)	(ksi)	(%)	(ksi)	(%)
Baseline design	126.5		-37		157.1	
High-strength design	92.1	-27.2%	-45.9	22.3%	136.3	-13.3%
Low-noise design	89.2	-29.4%	-35.3	-6.1%	113.8	-27.6%
Improved-bearing-contact low-noise design	95.6	-24.4%	-26.2	-30.6%	116.4	-25.9%
Formate design	76.2	-39.7%	-24.5	-34.6%	98.1	-37.6%
b) Gear fillet gages	Max Stress	Change	Min Stress	Change	Alt Stress	Change
	(ksi)	(%)	(ksi)	(%)	(ksi)	(%)
Baseline design	87.8		-34.6		118.4	
High-strength design	76.9	-12.4%	-21.3	-38.4%	87.2	-14.4%
Low-noise design	71.1	-19.0%	-35.3	-6.1%	113.8	-26.6%
Improved-bearing-contact low-noise design	56.2	-35.0%	-28.9	-16.5%	82.4	-30.4%
Formate design	64.2	-26.9%	-26.1	-24.7%	85.3	-27.9%
c) Pinion root gages	Max Stress	Change	Min Stress	Change	Alt Stress	Change
	(ksi)	(%)	(ksi)	(%)	(ksi)	(%)
Baseline design	33.0		-39.9		72.5	
High-strength design	41.1	24.7%	-76.4	-91.2%	110.3	52.3%
Low-noise design	41.0	24.2%	-70.9	77.5%	109.7	51.3%
Improved-bearing-contact low-noise design	57.5	74.2%	-54.3	35.9%	110.6	52.7%
Formate design	42.0	27.2%	-56.3	40.9%	93.0	28.3%
d) Gear root gages	Max Stress	Change	Min Stress	Change	Alt Stress	Change
	(ksi)	(%)	(ksi)	(%)	(ksi)	(%)
Baseline design	30.0		-67.3		92.0	
High-strength design	39.5	31.5%	-73.6	9.4%	107.2	16.5%
Low-noise design	29.6	-1.5%	-74.6	10.9%	94.9	3.3%
Improved-bearing-contact low-noise design	30.0	0.0%	-74.2	10.3%	97.3	5.7%
Formate design	42.0	0.6%	-56.3	-10.7%	83.7	-9.0%

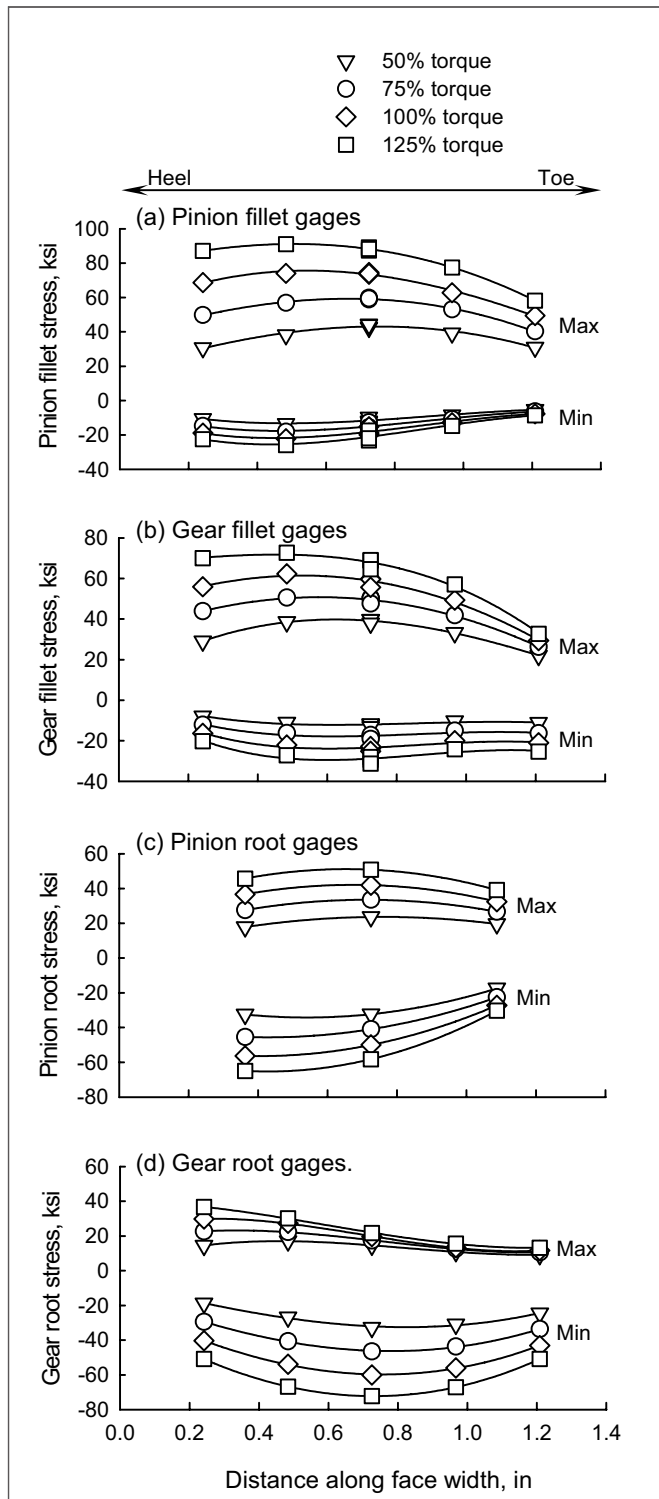


Figure 17—Effect of torque on the stress distribution along the gear tooth face width, static strain tests. Formate design only.

the Formate and low-noise designs (Table 2d).

Figure 17 depicts the strain results for the Formate design at all loads tested (50, 75, 100 and 125% torque). As expected, the figure shows a linear increase in stress with torque. The increase is greater at the heel, compared to the toe, for most cases.

Figure 18 compares the dynamic and static stresses for the pinion fillet and root gages for the Formate design at all loads tested. For the most part, the dynamic stresses were about the same—or sometimes less—than the static stresses. This shows a good design from the dynamic standpoint, with no penalties due to dynamic loads.

**Bevel tooth contact patterns.** As previously reported, the original low-noise designs showed a significant decrease in spiral bevel gear noise, vibration and tooth fillet stress (Refs. 1 and 2). However, a hard-line condition (concentrated wear lines) was present on the pinion tooth flank area for these designs. The improved-bearing-contact, low-noise design corrected this issue (Ref. 8). Figures 19 and 20 show close-up photographs of the pinion and gear, respectively, for the Formate design after completion of all tests to check tooth contact and meshing patterns. No hard-line conditions were found on the pinion and gear tooth flanks.


### Summary of Results

Studies to evaluate low-noise, Formate spiral bevel gears were performed. Experimental tests were conducted on the OH-58D helicopter main-rotor transmission in the NASA Glenn 500-hp helicopter transmission test stand. Formate spiral bevel gears were compared to the baseline OH-58D spiral bevel gear design, a high-strength design and previously tested low-noise designs. Noise, vibration and tooth strain tests were performed. The following results were obtained:

1) The Formate spiral bevel design showed a decrease in noise compared to the baseline OH-58D design (about 5 dB at 100% torque), but not as much reduction as previously tested, low-noise designs (about 16 dB at 100% torque). The bevel mesh sound power for the improved-bearing-contact, low-noise design was nearly constant with torque.

2) The Formate spiral bevel design gave the same benefit in reduced vibration—compared to the baseline OH-58D design—as that of the previously tested, low-noise designs. As with the noise test results, the vibration for the Formate design was nearly constant with torque.

3) The spiral bevel pinion tooth stresses for the Formate design showed a significant decrease compared to the baseline OH-58D design, even greater than previously tested high-strength and low-noise designs. Also, the gear stresses significantly decreased compared to the baseline OH-58D design. For the Formate design, the maximum stresses shifted toward the heel, compared to the center of the face width for the baseline, high-strength and previously tested low-noise designs. There was no apparent change in stresses due to dynamic effects for the Formate design.

4) No hard-line conditions were found on the pinion or gear tooth flanks for the Formate design. 



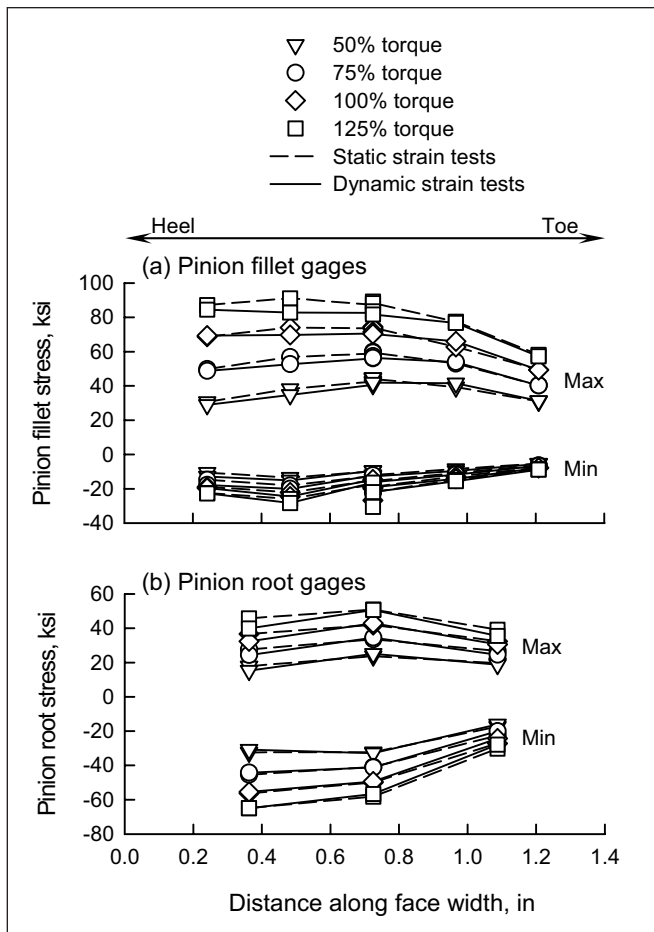


Figure 18—Comparison of static and dynamic strain tests. Formate design only.



Figure 19—Spiral-bevel pinion tooth contact after tests. Formated design.

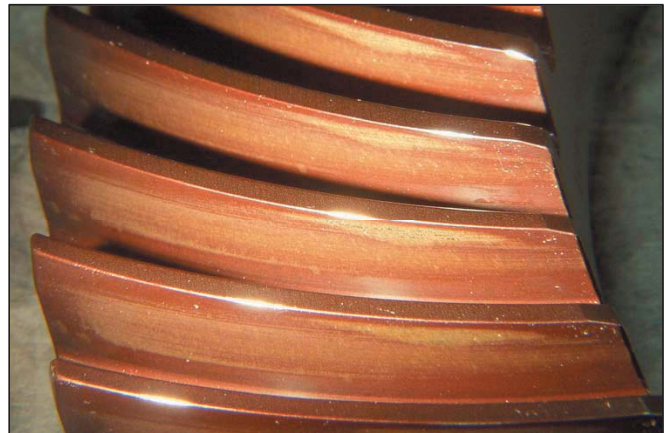


Figure 20—Spiral-bevel gear tooth contact after tests. Formated design.

## Acknowledgments

Technical tasks described in this document include tasks supported with shared funding by the U.S. rotorcraft industry and government under the NRTC/RITA Cooperative Agreement No. NCC2-9019, Advanced Rotorcraft Technology, January 1, 2001.

## References

1. Lewicki, D.G., R.F. Handschuh, Z.S. Henry and F.L. Litvin. "Improvements in Spiral-Bevel Gears to Reduce Noise and Increase Strength," *Proceedings of the 1994 International Gearing Conference*, Sep. 1994, pp. 341-346.
2. Lewicki, D.G., R.F. Handschuh, Z.S. Henry and F.L. Litvin. "Low-Noise, High-Strength, Spiral-Bevel Gears for Helicopter Transmissions," *AIAA Journal of Propulsion and Power*, Vol. 10, No. 3, May-Jun. 1994, pp. 356-361.
3. Litvin, F.L. and Y. Zhang. "Local Synthesis and Tooth Contact Analysis of Face-Milled Spiral Bevel Gears," NASA CR-4342, 1991.
4. Litvin, F.L., and A. Fuentes. *Gear Geometry and Applied Theory*, 2nd ed., Cambridge University Press, 2004.
5. Litvin, F.L., Y. Zhang and J. Chen. "User's Manual for Tooth Contact Analysis of Face-Milled Spiral Bevel Gears with Given Machine-Tool Settings," NASA CR-189093, 1991.
6. Litvin, F.L., C. Kuan and Y. Zhang. "Determination of Real Machine-Tool Settings and Minimization of Real Surface Deviation by Computer Inspection," NASA CR-4383, 1991.
7. Fuentes, A., F.L. Litvin, B.R. Mullins, R.L. Woods, R. F. Handschuh and D.G. Lewicki. "Design and Stress Analysis of Low-Noise Adjusted-Bearing-Contact Spiral Bevel Gears," *Proceedings of the International Conference on Gears*, Munich, Germany, Vol. 1, Mar. 2002, pp. 327-340.
8. Lewicki, D.G. and R.L. Woods. "Evaluation of Low-Noise, Improved-Bearing-Contact Spiral Bevel Gears," *Proceedings of the 59th American Helicopter Society Annual Forum*, Phoenix, AZ, May 2003.
9. Krenzer, T.J. "Face Milling or Face Hobbing," American Gear Manufacturers Association Paper No. 90FTM13, 1990.
10. Krenzer, T.J. "CNC Bevel Gear Generators and Flared Cup Formate Gear Grinding," American Gear Manufacturers Association Paper No. 91FTM1, 1991.
11. Litvin, F.L., Q. Fan and A. Fuentes. "Computerized

Design, Generation and Simulation of Meshing and Contact of Face-Milled Formate Cut Spiral Bevel Gears [Final Report],” NASA CR-2001-210894, ARL-CR-467, 2001.

12. Litvin, F.L., A. Fuentes, B.R. Mullins and R. Woods. “Computerized Design, Generation, Simulation of Meshing and Contact, and Stress Analysis of Formate Cut Spiral Bevel Gear Drives; Final Report,” NASA/CR-2003-212336, ARL-CR-525, 2003.

13. Scott, H.W. “Computer Numerical Control Grinding of Spiral Bevel Gears,” 1991, NASA CR-187175, AVSCOM TR-90-F-6.

14. Hirt, M.C.O. “Stress in Spur Gear Teeth and Their Strength as Influenced by Fillet Radius,” Ph.D. Dissertation, Technische Universitat Munchen, 1976, translated by the American Gear Manufacturers Association.

15. Drago, R.J. “Design Guidelines for High-Capacity Bevel Gear Systems,” *AE-15 Gear Design, Manufacturing and Inspection Manual*, Society of Automotive Engineers, 1990, pp. 105-121.

16. Winter, H., and M. Paul. “Influence of Relative Displacements Between Pinion and Gear on Tooth Root Stresses of Spiral Bevel Gears,” 1985, *Journal of Mechanisms Transmissions and Automation in Design*, Vol. 107, pp. 43-48.

*This article was originally published by the American Society of Mechanical Engineers (ASME) for the ASME 2007 International Design Engineering Technical Conferences & Computers and Information in Engineering Conference. It is republished here with the permission of ASME.*

**Dr. David Lewicki** is employed by the U.S. Army Research Laboratory's Vehicle Technology Directorate, located at the NASA Glenn Research Center at Lewis Field in Cleveland, OH. Since 1982, he has conducted analytical and experimental research in transmission, gearing and bearing areas for rotorcraft and turboprop drivetrain applications. His specific areas of research include face gears for helicopter transmissions; low-noise gears; gear crack propagation; gear diagnostics; engine disk crack detection; lubrication; transmission life; reliability predictions; and gear dynamics. Lewicki holds a Ph. D from Case Western Reserve University, has authored or co-authored 100 technical publications addressing the drive system area, and has been government manager for 36 contractor reports. He currently serves as an ASME Fellow, and previously worked as an editor for the *Journal of Mechanical Design*. He has also served as chairman of the ASME power transmission and gearing committee.

**Dr. Alfonso Fuentes** is a professor of mechanical engineering at the Polytechnic University of Cartagena (UPCT), and was formerly a visiting scholar at the Gear Research Center of the University of Illinois, Chicago (UIC), from 1999 to 2001. His areas of expertise include computerized development of improved gear transmissions for the rotorcraft, automotive and marine industries; development of enhanced computer models of gears for stress analysis; and the design of computer programs for generation and simulation of meshing of low-noise, stable-bearing-contact spiral bevel gears improved geometry. Fuentes is a member of both AGMA and ASME, and serves as associate editor of the *Journal of Mechanism and Machine Theory*, specializing in gears.

**Dr. Faydor L. Litvin** is an engineering distinguished emeritus professor at the University of Illinois, Chicago (UIC) and an honorable doctor at the University of Miskolc, Hungary. He has conducted research in the theory of gearing, transmission gear design, linkages and manipulators since 1946. Author of more than 350 publications containing 12 monographs, he graduated with distinction in 1937 from Leningrad Polytechnic University. He holds doctorates from Tomsk Polytechnic University (1944) and Leningrad Polytechnic University (1954). He is also the author or co-author of 22 certificates of inventions and four U.S. patents. Among many industry recognitions are: 12 TechBrief certificates of NASA, ASME Thomas A. Edison Patent Award; ASME Best Paper Award; and the Thomas Bernard Hall Prize Award of the Institution of Mechanical Engineers/UK. He is also an ASME fellow and former director of the Gear Research Center at UIC.

**Ron L. Woods** is employed by Bell Helicopter Textron in Fort Worth, TX, working in the Drive System Analysis Group since 1980. As a technical resource specialist, he is responsible for establishing best practices and for maintaining the state-of-the-art in analytical tools and methods for gear system design and analysis. Specifically, he has been involved in the drive system design of many Bell Helicopter models such as the AH-1W, H-1 upgrade, OH-58D, 407, 427, 430 and, most recently, the 429. He has also been involved in the design of the tiltrotor models V-22, BA609 and the Eagle Eye UAV. Woods holds a Bachelor of Science in mechanical engineering from the University of Texas at Austin, and is a licensed professional engineer in Texas.